Optical Materials 169 (2026) 117620

Contents lists available at ScienceDirect

Optical Materials

journal homepage: www.elsevier.com/locate/optmat

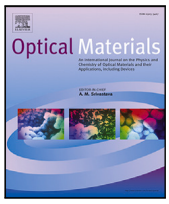

Research article

Bulk and surface-scattering loss measurements of CeF_3 crystals at 532 nm via cavity ring down spectroscopy

Michail Xygkis [a,b], Encarnación G. Víllora [c], George E. Katsoprinakis [a], Kiyoshi Shimamura [c], T. Peter Rakitzis [a,b,*]

[a] Institute for Electronic Structure and Lasers (IESL), FO.R.T.H., Heraklion, Greece
[b] University of Crete - Dept. of Physics, Heraklion, Greece
[c] National Institute for Materials Science (NIMS), Tsukuba, Japan

ARTICLE INFO

Keywords:
Magneto-optic crystal
Cerium Fluoride
CeF_3
Scattering losses

ABSTRACT

CeF_3 is a relatively new magneto-optical crystal with a wide transparency window (down to 300 nm) and an outstanding Verdet constant in the UV and visible spectral regions. The high transmittance of this fluoride in the visible was recently demonstrated in cavity ring-down measurements at 532 nm, where bulk losses of no more than 0.004 cm^{-1} were measured (Xygkis et al., 2023), although the total losses were significantly higher and dominated by surface scattering. Here, we show that reducing surface scattering and improving crystal quality, by suppressing the random formation of hexagonal micro-void defects in the bulk of the crystal which cause bulk scattering, leads to significantly reduced overall losses. Bulk loss coefficients as low as 0.002 cm^{-1} at 532 nm, half the previously measured value, are achieved in select samples, which is the current state-of-the-art in high-quality CeF_3 single crystals. Further elimination of micro-voids in the bulk is expected to further improve transmittance. Compared to other magneto-optical crystals and glasses, the present CeF_3 crystals achieve the highest values of the *Figure of Merit* (FoM) we have defined for both single-pass and multi-pass (optical cavity) applications.

0. Introduction

Cavity Ring-Down Spectroscopy (CRDS) is widely used for sensitive absorption measurements and is a well-established method for the detection of small optical losses (<1%) in gaseous, liquid, thin-film and transparent bulk samples [1–10], as well as for the measurement of polarimetric [11–18] and ellipsometric angles of samples [19–22]. Recently, our group has used the CRDS technique for the precise and sensitive determination of optical losses in transparent crystals, with an emphasis on evaluating their performance as magneto-optical (M-O) crystals [23], particularly for optical cavity applications.

This technique allows for the evaluation of both uncoated and anti-reflection-(AR)-coated crystals. For non-AR-coated crystals, the alignment is fine-tuned so that the incident light beam is normal to the crystal surfaces, thus ensuring that surface reflections are confined within the cavity and along the beam path, effectively eliminating reflection losses.

Using this method, we have reported measurements on the absorption losses for various M-O crystals and glasses, namely terbium gallium garnet (TGG, $Tb_3Ga_5O_{12}$), terbium gallium phosphate (TGP, a Tb-based phosphate glass composed of 20% Tb_2O_3, 15% Ga_2O_3, and 65% P_2O_5), potassium terbium fluoride (KTF, KTb_3F_{10}), fused silica (FS, SiO_2), and cerium fluoride (CeF_3).

To assess the performance of each crystal, a *Figure of Merit* (FoM) was defined, with particular emphasis on multi-pass applications (*e.g.*, optical cavity), which depends on the surface and bulk losses of the crystal (and hence on its length) and its Verdet constant [23]. The conclusion of that study was that CeF_3 exhibited a – very desirable – combination of very low absorption and high Verdet constant [24], but its performance was limited by surface scattering losses. Consequently, for certain applications, particularly those in which short crystal lengths would suffice, other M-O materials (particularly TGP glass) outperformed CeF_3, despite the very low absorption losses of the latter.

In this work, high-quality CeF_3 crystals were grown using an established growth process. Taking extra care with surface preparation and cleaning, we achieved a significant improvement in surface quality: from the previously estimated level of ~0.5%, surface scattering was reduced to ~0.12%, which is on par with the minimum in surface scattering observed across all crystal measurements, even with the highest

* Corresponding author at: Institute for Electronic Structure and Lasers (IESL), FO.R.T.H., Heraklion, Greece.
E-mail address: ptr@iesl.forth.gr (T. Peter Rakitzis).

https://doi.org/10.1016/j.optmat.2025.117620
Received 31 August 2025; Received in revised form 3 October 2025; Accepted 17 October 2025
Available online 24 October 2025
0925-3467/© 2025 The Authors. Published by Elsevier B.V. This is an open access article under the CC BY license (http://creativecommons.org/licenses/by/4.0/).

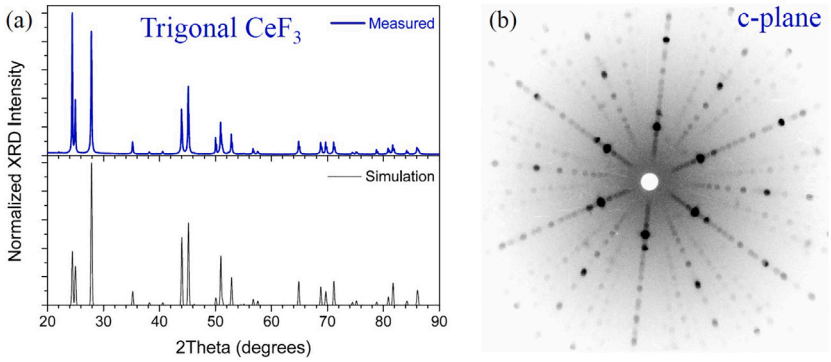

Fig. 1. (a) Powder X-ray diffraction pattern of grown CeF_3 and the trigonal reference ICSD-code #56773. (b) Back-reflection Laue pattern of a c-oriented crystal.

surface quality optics at our disposal, and is probably limited by dust accumulation on the surfaces. Consequently, the total observed optical losses were reduced from 0.7% [23] to 0.16%, still dominated by surface scattering, and followed by bulk losses, which are mainly due to bulk scattering at residual micro-void defects. Thus, we were able to determine that the absorption of CeF_3 is no more than $0.002\,cm^{-1}$ at 532 nm. Further elimination of bulk defect formation during the growth process will lead to even higher transmittance CeF_3 crystals. However, we can already stress that the combination of low surface scattering and low bulk losses make CeF_3 an excellent magneto-optical crystal in the visible. The preparation and characteristics of the CeF_3 crystals are described in detail in Section 1.

To facilitate the comparison among the current and previous CeF_3 crystals, and the other M-O materials, in Section 3 we calculate both the multi-pass-oriented FoM discussed above, as well as the commonly used single-pass M-O FoM [25,26], assuming low to moderate optical power applications where thermal effects can be ignored [27]. In light of these results, we conclude that CeF_3 can be considered the most suitable M-O crystal for both single-pass and multi-pass applications in the visible part of the spectrum (experiments performed at 532 nm), due to its combination of low optical losses and high Verdet constant. We also note that the crystals used in this work, although state-of-the-art, still show scattering (and/or absorption) at defects in the bulk. Therefore, the potential of the CeF_3 material has not been exhausted and further improvements of the CeF_3 properties are expected upon reduction or elimination of the bulk scattering centers.

1. CeF_3 single-crystal discs preparation

A high-quality CeF_3 single crystal was grown by the Bridgman technique as explained in a previous publication [28]. The trigonal phase of grown CeF_3, with space group P-3c1, was confirmed by X-ray powder diffraction using a Rigaku MiniFlex600 equipped with a Cu-target. The measured pattern is shown in comparison with the simulated one of the database, ICSD-code #56773, in Fig. 1(a).

Since this crystal is uniaxial, it was oriented along the optical axis by back-reflection Laue diffraction (see the 6-fold symmetry in Fig. 1(b)) and cut into thick *c*-oriented plates of three different thicknesses (with approximate lengths 1, 2, and 5 mm). Subsequently, these were shaped into discs of 8 mm in diameter. After lapping both end surfaces, these were fine processed by chemical–mechanical polishing (CMP) using a 1PM52-1 Logitech precision polishing machine. The surface of polished CeF_3 single crystals was evaluated by coherent scanning interferometry (CSI) using a Hitachi VS1800 Nano 3D optical interferometer. Polishing and surface evaluation were alternatively iterated until the absence of scratches over the whole surface could be confirmed.

Optical-grade polishing of end surfaces is essential to minimize the optical losses caused by surface scattering. As CeF_3 is a non-hygroscopic compound, a standard water-based silica slurry was used for CMP. The quality of CMP polished CeF_3 single crystals evaluated by CSI on the narrow ($12.8 \times 12.8\ \mu m^2$) and wide (>8 mm^2, whole surface) ranges is shown in the examples of Fig. 2(a) and (b), respectively. The arithmetic mean roughness, R_a, and the root mean square roughness, R_q, were as small as 2.05 Å and 2.60 Å, respectively, with a peak-to-valley (9.69 Å & −9.86 Å) total roughness, R_t, of 19.55 Å and an average of 0.03 Å. This excellent surface polishing was further confirmed by the complete absence of scratches over the whole surface, despite being a relatively soft fluoride compared to oxides. These results prove that the optical-grade polishing of present CeF_3 is comparable to that of optical-grade fused-silica, and, therefore, their surface losses, S, can be considered as equivalent.

On the other hand, as reflection losses are not evident by naked eye in the case of fused-silica, the 532 nm laser beam scattering observed in the case of CeF_3 in current measurements (see Fig. 5) can be attributed to bulk defects. In general, CeF_3 crystals are well-known to exhibit a milky appearance due to a large density of defects [28], and only high-quality samples, like the present ones, are seemingly scattering-free, as the path of laser beams is barely observable through the bulk of the crystal. Nevertheless, even the latter have been shown to possess a low density of bulk defects, namely flat hexagonal voids in the *c*-plane [29]. These regularly shaped hexagons are ultra-thin ($\ll \mu m$), frequently of submicron size and line up, seldom reaching a diameter of several microns, as shown in the optical microscope photographs of Fig. 3. The origin of these micro-voids is attributed to the formation of bubbles in the molten state due to the extraordinarily high vapor pressure of CeF_3 at the melting point (on the order of 10^{-2} atm [30], and evidenced by intense evaporation from the melt), so a growth hot zone with small thermal gradients was targeted to prevent the melt overheating. Large bubbles can move through the low-viscosity melt, leading to intense evaporation. In contrast, smaller ones remain trapped inside the crystal during the solidification process, their shape being determined by the difference in surface tension on different crystal planes. While the appearance of bubbles cannot be avoided at the melting of CeF_3, the average density of voids is expected to decrease with shallow thermal gradients and reduced overheating. Therefore, it is assumed that the bulk scattering observed in current experiments occurs at these residual voids. This hypothesis is further supported by the fact that observed scattering is inhomogeneous and varies from sample to sample, in good accordance with the random distribution of micro-voids. Since the purpose of the present characterization of CeF_3 using the CRDS technique is to establish an upper limit for the absorption coefficient, a sample with minimal optical losses, *i.e.*, with minimum bulk scattering, was selected.

2. CRDS setup and results

The experimental setup is described in detail in [23]. The optical cavity consists of two high-reflectivity (HR) mirrors, $R_1 = R_2 = R = 0.998$ (Layertec GmbH), and has a length $L_c = 50$ cm (we define the length of a two-mirror cavity as twice the separation between the

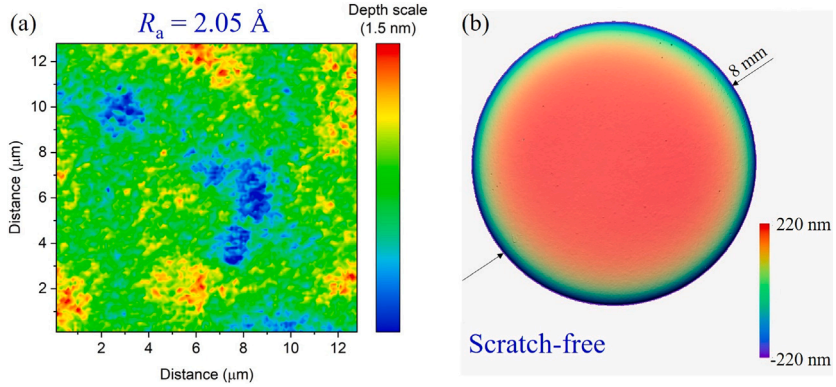

Fig. 2. CSI images of CMP fine-polished CeF_3 - (a) narrow 12.8×12.8 μm^2 range and (b) whole 8 mm in diameter surface.

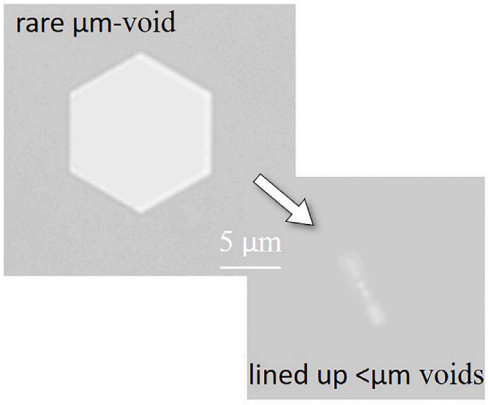

Fig. 3. Optical microscope photographs of scattering centers: a rare large micro-size hexagonal void and common lined up submicron hexagonal voids.

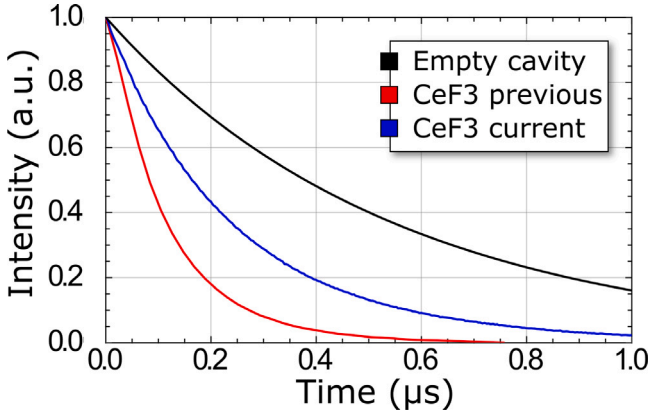

Fig. 4. Ring-down traces for the previous and current CeF_3 crystals at 532 nm. The increased ring-down time of the latter indicates its reduced optical losses (see Section 1).

cavity mirrors). The laser source operates at a wavelength $\lambda = 532$ nm (microchip laser, 1.3 ns pulse width, 1 kHz repetition rate, 20 μJ pulse energy). The M-O crystals were placed inside the cavity on a precision optic mount, which allowed micrometric alignment adjustments. The crystals were aligned so that their input/output surfaces were perpendicular to the beam path, ensuring that surface reflections remained confined within the cavity, thus eliminating surface reflection losses (but not surface scattering losses, which cannot be eliminated in this manner).

The single-pass losses of an intracavity crystal sample, L_{sp}, are determined using standard cavity ring-down theory [1]:

$$L_{s\text{-}p} = \frac{\tau_{rt}}{2}\left(\frac{1}{\tau_1} - \frac{1}{\tau_0}\right), \quad (1)$$

where $\tau_{rt} = L_c/c$ is the cavity round-trip time, τ_0 is the ring-down time of the empty cavity, and τ_1 is the ring-down time of the cavity containing the crystal sample. This formula is valid for $L_{s\text{-}p} \ll 1$. $L_{s\text{-}p}$ has two main contributions: (a) bulk losses (due to absorption and bulk scattering), and (b) surface losses (due to scattering from surface imperfections and/or dust, given that we have eliminated surface reflections, as discussed above). The single-pass losses can also be expressed as:

$$L_{s\text{-}p} = 1 - e^{-\kappa d}(1 - S), \quad (2)$$

where d is the crystal length, κ is the bulk loss coefficient (containing both absorption and bulk scattering contributions), and S represents the surface scattering losses. Since pure, single-crystal CeF_3 absorption is expected to be very low in the spectral region under study, κ should be attributed mainly to bulk scattering.

In [23], we first studied optical-grade polished fused silica (FS) crystals, to establish a baseline for surface scattering losses in the case of minimal bulk absorption. The total FS crystal optical loss was found to be $S = 0.12\%$ per pass, essentially attributed entirely to surface scattering. Indeed, using Eqs. (1) and (2) and $\kappa_{FS} \simeq 10^{-5}\,cm^{-1}$ [31], for a $d = 1$ cm fused silica crystal we get $1 - e^{-\kappa d} \simeq 10^{-5}$, which is negligible compared to the measured crystal losses. To further verify that measured losses were indeed due to scattering rather than to *e.g.*, misalignment, a thin uncoated BK7 window was placed in the cavity at Brewster's angle. This configuration is much less sensitive to alignment, and measured losses were virtually identical in both cases, confirming that surface scattering was the main source of losses for fused silica and BK7 at 532 nm.

We also measured the losses for two CeF_3 crystals of different lengths (2.2 mm and 6.2 mm) and found no discernible difference in their overall losses per pass, within experimental error. The total per-pass loss was found to be $0.70\% \pm 0.05\%$ for both crystals, and the bulk loss coefficient, $\kappa_{CeF_3} \leq 0.004\,cm^{-1}$.

In this work, as described in Section 1, we used a CeF_3 sample with minimal density of bulk defects and entirely scratch-free surface polishing, which showed markedly lower total losses compared to the former, randomly chosen CeF_3 samples. The ring-down traces for the CeF_3 crystals in the two cases are shown in Fig. 4. From the ring-down measurements, the total single-pass loss of the current crystal was found to be $0.16\% \pm 0.05\%$, significantly lower than the previously measured value of $0.70\% \pm 0.05\%$. Having established the high quality of the polished crystal surfaces, we assume its surface scattering losses are comparable to those of fused silica ($S = 0.12\%$, see Section 1), and we calculate the new bulk loss coefficient,

$$\kappa_{CeF_3} \leq 0.0020 \pm 0.0003\,cm^{-1} \quad (3)$$

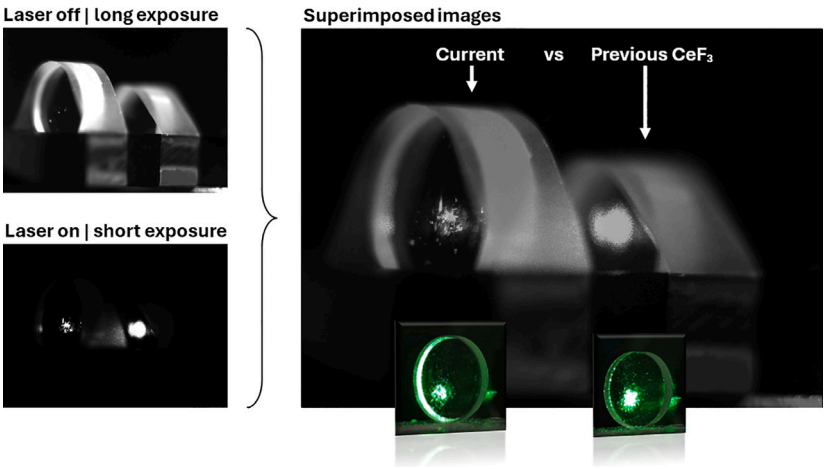

Fig. 5. Scattering of 532 nm light from previous and current CeF_3 crystal samples, under identical experimental conditions. Here, the short exposure image showing the scattering effect is superimposed with a long exposure image taken with the laser off, for better visibility and clarity. The current sample shows notably reduced scattering due to its lower density of bulk defects (see Section 1). Further elimination of residual bulk defects during the growth process will result to even lower optical losses.

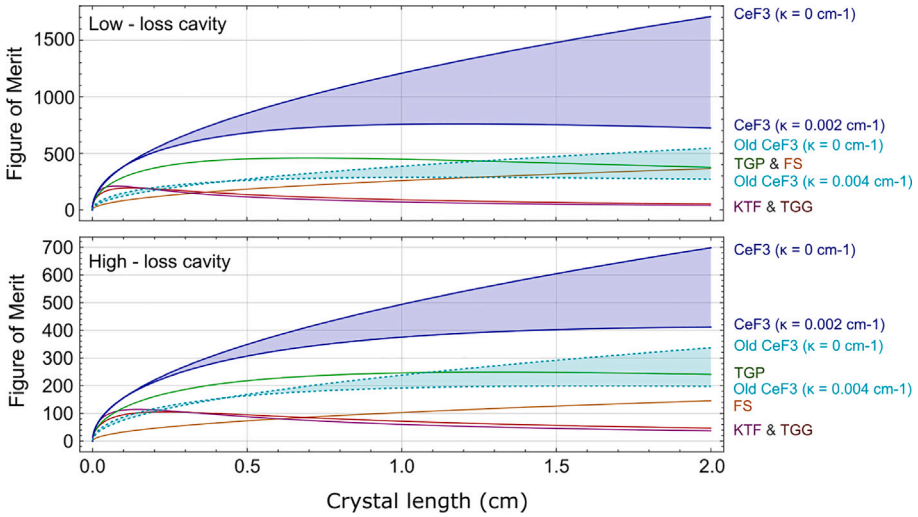

Fig. 6. Figure of Merit for optical cavity applications. **Top:** Low-loss cavity with $T_{IC} = 0.997$ and $R = 0.9995$. **Bottom:** High-loss cavity with $T_{IC} = 0.993$ and $R = 0.9995$. CeF_3 curves are plotted for the lower and upper bounds of the bulk loss coefficient 2σ confidence interval (0 and $0.0020\,cm^{-1}$, respectively) and for surface scattering losses of $S = 0.120\% - 0.164\%$ per pass (for $\kappa = 0 - 0.0020\,cm^{-1}$ respectively). We note that a minimal value of ~0.12% per pass for surface scattering is common for all crystals under study and is mainly due to small dust particulates settling on the crystal surfaces, and not fundamentally due to the quality of the surface, as the experiments are not performed in a clean room or in vacuum.

3. Discussion

The optical losses and Verdet constants of M-O crystals are critical parameters that determine their suitability for applications such as optical isolation or Cavity Ring-Down Polarimetry (CRDP). In [23] and in this work we focused on CeF_3 crystals, which are of particular interest for applications in the visible part of the spectrum, due to their low absorption losses and high Verdet constant. By using a state-of-the-art growth process and applying high quality surface polishing techniques, we minimized both bulk and surface scattering, and, from the grown crystals, we selected those CeF_3 samples which had the lowest residual bulk defect densities. We measured the total single-pass optical losses of few-mm-long crystals, and we found that, compared to [23], losses were reduced from $0.70\% \pm 0.05\%$, to $0.16\% \pm 0.05\%$ in this work. Thus, a new minimum was established for the value of the bulk loss coefficient of CeF_3: $\kappa_{CeF_3} = 0.0020 \pm 0.0003\,cm^{-1}$.

To compare sample quality, in Fig. 5 we show pictures of the laser beam scattering on one of the previously used CeF_3 crystals versus the current one, under identical experimental conditions. Although the improvement is evident and the CeF_3 sample demonstrates very low overall optical losses, it is also clear that visible scattering can still be observed. Given this observation, and considering that absorption of pure CeF_3 is projected to be exceedingly low in the spectral region under study due to the absence of nearby electronic transitions, an even lower loss coefficient than that of Eq. (3) is expected upon reduction or elimination of residual scattering centers.

In Fig. 6, we extend the Figure of Merit (FoM) plot from [23] to include the current CeF_3 crystal results, so that its performance as an intra-cavity M-O element can be compared to the other M-O crystals. We remind here the formula for the FoM, as defined in [23] for multi-pass/intra-cavity applications:

$$\text{FoM} = \frac{(V\,B\,d)^{\frac{1}{2}}}{(1 - R\,T_{IC}\,e^{-\kappa d}(1-S))^{3/2}} \qquad \text{(multi-pass)} \tag{4}$$

where R is the total reflection coefficient of all cavity mirrors, T_{IC} is the combined transmission coefficient of all intra-cavity optics other

Table 1
Single-pass FoM = V/κ, for the various M–O crystals at 532 nm.

Crystal	V (rad/T m)	κ (m^{-1})	FoM (rad/T)
TGG	198	2.89	66.0
TGP	106	0.35	311.8
KTF	107	1.92	55.7
Previous CeF_3	171	0.40	427.5
Current CeF_3	171	0.20	855.0

than the crystal, V is the Verdet constant, d the length, and S the scattering losses per pass of the M-O crystal, and B the strength of the magnetic field applied parallel to the light-propagation axis. For more details on the definition of this FoM, the reader is referred to [23]. The FoM is plotted for optical cavity setups with both low and high losses (other than the losses of the M-O crystal). It can be seen that the current CeF_3 crystal outperforms all other M-O crystals by a significant margin, in the spectral region under study, across the whole crystal length range. In particular, CeF_3 surpasses the TGP glass, which in the previous investigation had a comparable FoM, particularly for shorter crystals.

Finally, using the values from [23] for the Verdet constant and absorption coefficient of TGG, TGP, and KTF at 532 nm, we calculate the single-pass FoM commonly quoted for M-O crystals, for single-pass applications [25]:

$$\text{FoM} = \frac{V}{\kappa} \qquad \text{(single-pass)} \tag{5}$$

The results are summarized in Table 1. From the calculated values, CeF_3 is confirmed to outperform the other well-known M-O crystals we studied, also for single-pass applications.

Conclusions

We report improved CeF_3 crystals with negligible surface-scattering losses and bulk scattering, and therefore absorption losses of no more than 0.002 cm^{-1}. The reduction in bulk scattering is due to a decrease in micro-voids, which is favored by low thermal gradients and minimum overheating at the molten state. Thanks to these improvements, CeF_3 crystals have the highest figure of merit for magneto-optical crystals in the visible and near UV, both for single-pass and multi-pass (e.g., optical cavity) applications. The present CeF_3 crystals exhibit, to the best of our knowledge, the highest optical quality to date. A further decrease in optical losses implies the elimination of micro-voids, i.e. a suppression of bubble formation. Given the extremely high vapor pressure of CeF_3 at its melting point, growth under high pressure is impractical. Instead, the growth with a flux at a temperature well below the melting point seems a reasonable approach to achieve further improvements in crystalline quality.

CRediT authorship contribution statement

Michail Xygkis: Writing – original draft, Methodology, Investigation, Formal analysis, Data curation. **Encarnación G. Víllora:** Writing – review & editing, Resources, Methodology, Investigation, Formal analysis, Data curation, Conceptualization. **George E. Katsoprinakis:** Writing – review & editing, Visualization, Software, Methodology, Formal analysis, Data curation. **Kiyoshi Shimamura:** Writing – review & editing, Resources, Methodology, Investigation, Formal analysis, Data curation. **T. Peter Rakitzis:** Writing – review & editing, Supervision, Project administration, Methodology, Funding acquisition, Conceptualization.

Declaration of competing interest

The authors declare that they have no known competing financial interests or personal relationships that could have appeared to influence the work reported in this paper.

Acknowledgments

This work was partially supported by the Hellenic Foundation for Research and Innovation (HFRI) and the General Secretariat for Research and Technology (GSRT), under grant agreement No. HFRI-FM17-3709 (project NUPOL), and by the GSRT within the framework of the National Recovery and Resilience Plan Greece 2.0, funded by the European Union – NextGenerationEU, under the call RESEARCH-CREATE-INNOVATE (Implementation body: MIA RI), under grant agreement TAEΔK-06187 (project TEARSENSE).

Data availability

Data will be made available on request.

References

[1] Daniele Romanini, Irène Ventrillard, Guillaume Méjean, Jérôme Morville, Erik Kerstel, Introduction to cavity enhanced absorption spectroscopy, in: Gianluca Gagliardi, Hans-Peter Loock (Eds.), Cavity-Enhanced Spectroscopy and Sensing, Springer, Berlin, Heidelberg, ISBN: 978-3-642-40003-2, 2014, pp. 1–60, http://dx.doi.org/10.1007/978-3-642-40003-2_1, (visited on 03/13/2025).

[2] D. Romanini, K.K. Lehmann, Ring-down cavity absorption spectroscopy of the very weak HCN overtone bands with six, seven, and eight stretching quanta, J. Chem. Phys. 99 (9) (1993) 6287–6301, http://dx.doi.org/10.1063/1.465866, ISSN: 0021-9606, 1089-7690. URL: http://aip.scitation.org/doi/10.1063/1.465866. (visited on 02/16/2023).

[3] Giel Berden, Peeters Rudy, Gerard Meijer, Cavity ring-down spectroscopy: Experimental schemes and applications, Int. Rev. Phys. Chem. (ISSN: 0144-235X) 19 (4) (2000) 565–607, http://dx.doi.org/10.1080/014423500750040627, (visited on 03/21/2025).

[4] Piotr Zalicki, Richard N. Zare, Cavity ring-down spectroscopy for quantitative absorption measurements, J. Chem. Phys. 102 (7) (1995) 2708–2717, http://dx.doi.org/10.1063/1.468647, ISSN: 0021-9606, 1089-7690. URL: http://aip.scitation.org/doi/10.1063/1.468647. (visited on 02/16/2023).

[5] Roger D. van Zee, Joseph T. Hodges, J. Patrick Looney, Pulsed, single-mode cavity ringdown spectroscopy, Appl. Opt. (ISSN: 2155-3165) 38 (18) (1999) 3951–3960, http://dx.doi.org/10.1364/AO.38.003951, URL: https://opg.optica.org/ao/abstract.cfm?uri=ao-38-18-3951. (visited on 06/05/2023).

[6] Richard Engeln, Gert von Helden, André J.A. van Roij, Gerard Meijer, Cavity ring down spectroscopy on solid C60, J. Chem. Phys. (ISSN: 0021-9606) 110 (5) (1999) 2732–2733, http://dx.doi.org/10.1063/1.477997, (visited on 03/21/2025).

[7] George A. Marcus, H. Alan Schwettman, Cavity ringdown spectroscopy of thin films in the mid-infrared, Appl. Opt. 41 (24) (2002) 5167, http://dx.doi.org/10.1364/AO.41.005167, ISSN: 0003-6935, 1539-4522. URL: https://opg.optica.org/abstract.cfm?URI=ao-41-24-5167. (visited on 03/21/2025).

[8] Georgiy Vaschenko, Yogesh Godwal, Carmen S. Menoni, Claude Montcalm, Richard Blacker, Daniel Siegfried, Characterization of thin-film losses with a synchronously pumped ringdown cavity, Appl. Opt. 42 (22) (2003) 4584, http://dx.doi.org/10.1364/AO.42.004584, ISSN: 0003-6935, 1539-4522. URL: https://opg.optica.org/abstract.cfm?URI=ao-42-22-4584. (visited on 03/21/2025).

[9] C. Cotirlan, C. Logofatu, Adrian Rizea, M.F. Lazarescu, Angle-resolved evanescent-wave cavity ring-down spectroscopy for thin film-solid interface characterization, Optoelectron. Adv. Mater. Rapid Commun. 5 (2011) 709–714.

[10] Binghua Cai, Bincheng Li, Yaowei Wei, Yanling Han, Tianmin Wang, Jing Wang, Hao Cui, Accurate loss measurement of optical bulk materials with the pulsed cavity ring-down technique, Opt. Express (ISSN: 1094-4087) 32 (23) (2024) 40375–40385, http://dx.doi.org/10.1364/OE.537747, URL: https://opg.optica.org/oe/abstract.cfm?uri=oe-32-23-40375. (visited on 04/22/2025).

[11] Thomas Müller, Kenneth B. Wiberg, Patrick H. Vaccaro, Cavity ring-down polarimetry (CRDP): A new scheme for probing circular birefringence and circular dichroism in the gas phase, J. Phys. Chem. A 104 (25) (2000) 5959–5968, http://dx.doi.org/10.1021/jp000705n, ISSN: 1089-5639, 1520-5215. URL: https://pubs.acs.org/doi/10.1021/jp000705n. (visited on 02/16/2023).

[12] Thomas Müller, Kenneth B. Wiberg, Patrick H. Vaccaro, James R. Cheeseman, Michael J. Frisch, Cavity ring-down polarimetry (CRDP): Theoretical and experimental characterization, J. Opt. Soc. Am. B 19 (1) (2002) 125, http://dx.doi.org/10.1364/JOSAB.19.000125, ISSN: 0740-3224, 1520-8540. URL: https://opg.optica.org/abstract.cfm?URI=josab-19-1-125. (visited on 02/16/2023).

[13] Dimitris Sofikitis, Lykourgos Bougas, Georgios E. Katsoprinakis, Alexandros K. Spiliotis, Benoit Loppinet, T. Peter Rakitzis, Evanescent-wave and ambient chiral sensing by signal-reversing cavity ringdown polarimetry, Nature (ISSN: 1476-4687) 514 (7520) (2014) 76–79, http://dx.doi.org/10.1038/nature13680, URL: https://www.nature.com/articles/nature13680. (visited on 02/14/2023).

[14] A.K. Spiliotis, M. Xygkis, E. Klironomou, E. Kardamaki, G.K. Boulogiannis, G.E. Katsoprinakis, D. Sofikitis, T.P. Rakitzis, Gas-phase optical activity measurements using a compact cavity ringdown polarimeter, Laser Phys. (ISSN: 1555-6611) 30 (7) (2020) 075602, http://dx.doi.org/10.1088/1555-6611/ab8d2e, (visited on 02/16/2023).

[15] A.K. Spiliotis, M. Xygkis, E. Klironomou, E. Kardamaki, G.K. Boulogiannis, G.E. Katsoprinakis, D. Sofikitis, T.P. Rakitzis, Optical activity of lysozyme in solution at 532 nm via signal-reversing cavity ring-down polarimetry, Chem. Phys. Lett. (ISSN: 0009-2614) 747 (2020) 137345, http://dx.doi.org/10.1016/j.cplett.2020.137345, URL: https://www.sciencedirect.com/science/article/pii/S0009261420302608. (visited on 02/16/2023).

[16] Jim C. Visschers, Oleg Tretiak, Dmitry Budker, Lykourgos Bougas, Continuous-wave cavity ring-down polarimetry, J. Chem. Phys. (ISSN: 0021-9606) 152 (16) (2020) 164202, http://dx.doi.org/10.1063/5.0004476, (visited on 05/09/2023).

[17] Dang-Bao-An Tran, Katherine M. Manfred, Robert Peverall, Grant A.D. Ritchie, Continuous-wave cavity-enhanced polarimetry for optical rotation measurement of chiral molecules, Anal. Chem. 93 (13) (2021) 5403–5411, http://dx.doi.org/10.1021/acs.analchem.0c04651, ISSN: 0003-2700, 1520-6882. URL: https://pubs.acs.org/doi/10.1021/acs.analchem.0c04651. (visited on 02/16/2023).

[18] Lykourgos Bougas, Joseph Byron, Dmitry Budker, Jonathan Williams, Absolute optical chiral analysis using cavity-enhanced polarimetry, Sci. Adv. 8 (22) (2022) eabm3749, http://dx.doi.org/10.1126/sciadv.abm3749, URL: https://www.science.org/doi/10.1126/sciadv.abm3749. (visited on 02/16/2023).

[19] Vassilis Papadakis, Michael A. Everest, Katerina Stamataki, Stelios Tzortzakis, Benoit Loppinet, T. Peter Rakitzis, Development of cavity ring-down ellipsometry with spectral and submicrosecond time resolution, in: Instrumentation, Metrology, and Standards for Nanomanufacturing, Optics, and Semiconductors V, Vol. 8105, SPIE, 2011, pp. 104–112, http://dx.doi.org/10.1117/12.903053, URL: https://www.spiedigitallibrary.org/conference-proceedings-of-spie/8105/81050L/Development-of-cavity-ring-down-ellipsometry-with-spectral-and-submicrosecond/10.1117/12.903053.full. (visited on 03/21/2025).

[20] Dimitris Sofikitis, Katerina Stamataki, Michael A. Everest, Vassilis Papadakis, Jean-Louis Stehle, Benoit Loppinet, T. Peter Rakitzis, Sensitivity enhancement for evanescent-wave sensing using cavity-ring-down ellipsometry, Opt. Lett. 38 (8) (2013) 1224, http://dx.doi.org/10.1364/OL.38.001224, ISSN: 0146-9592, 1539-4794. URL: https://opg.optica.org/abstract.cfm?URI=ol-38-8-1224. (visited on 02/13/2025).

[21] Katerina Stamataki, Vassilis Papadakis, Michael A. Everest, Stelios Tzortzakis, Benoit Loppinet, T. Peter Rakitzis, Monitoring adsorption and sedimentation using evanescent-wave cavity ringdown ellipsometry, Appl. Opt. (ISSN: 2155-3165) 52 (5) (2013) 1086–1093, http://dx.doi.org/10.1364/AO.52.001086, URL: https://opg.optica.org/ao/abstract.cfm?uri=ao-52-5-1086. (visited on 02/13/2025).

[22] D. Sofikitis, A.K. Spiliotis, K. Stamataki, G.E. Katsoprinakis, L. Bougas, P.C. Samartzis, B. Loppinet, T.P. Rakitzis, M. Surligas, S. Papadakis, Microsecond-resolved SDR-based cavity ring down ellipsometry, Appl. Opt. (ISSN: 2155-3165) 54 (18) (2015) 5861–5865, http://dx.doi.org/10.1364/AO.54.005861, URL: https://opg.optica.org/ao/abstract.cfm?uri=ao-54-18-5861. (visited on 02/16/2023).

[23] Michalis Xygkis, Artemis N. Linaraki, Eirini N. Toutoudaki, Georgios E. Katsoprinakis, T. Peter Rakitzis, Absorption coefficients and scattering losses of TGG, TGP, KTF, FS, and CeF_3 magneto-optical crystals in the visible via cavity ring-down spectroscopy, Appl. Opt. (ISSN: 2155-3165) 62 (29) (2023) 7730–7735, http://dx.doi.org/10.1364/AO.496780, URL: https://opg.optica.org/ao/abstract.cfm?uri=ao-62-29-7730. (visited on 01/10/2024).

[24] Encarnación G. Víllora, Kiyoshi Shimamura, Gustavo R. Plaza, Ultraviolet-visible optical isolators based on CeF_3 faraday rotator, J. Appl. Phys. (ISSN: 0021-8979) 117 (23) (2015) 233101, http://dx.doi.org/10.1063/1.4922497, (visited on 03/18/2025).

[25] Valentyn Vasyliev, Encarnacíon G. Villora, Masaru Nakamura, Yoshiyuki Sugahara, Kiyoshi Shimamura, UV-visible faraday rotators based on rare-earth fluoride single crystals: $LiREF_4$ (RE=Tb, Dy, Ho, Er and Yb), PrF_3 and CeF_3, Opt. Express (ISSN: 1094-4087) 20 (13) (2012) 14460–14470, http://dx.doi.org/10.1364/OE.20.014460, URL: https://opg.optica.org/oe/abstract.cfm?uri=oe-20-13-14460. (visited on 03/21/2025).

[26] Christoph Tyborski, Muhammad T. Hassan, Thomas Flisgen, Max Schiemangk, Andreas Wicht, Extensive study of magneto-optical and optical properties of $Cd_{1-x}Mn_xTe$ between 675 and 1025 nm, AIP Adv. (ISSN: 2158-3226) 13 (1) (2023) 015213, http://dx.doi.org/10.1063/5.0130535, (visited on 03/20/2025).

[27] David Vojna, Ondřej Slezák, Antonio Lucianetti, Tomáš Mocek, Verdet constant of magneto-active materials developed for high-power faraday devices, Appl. Sci. (ISSN: 2076-3417) 9 (15) (2019) 3160, http://dx.doi.org/10.3390/app9153160, URL: https://www.mdpi.com/2076-3417/9/15/3160. (visited on 03/20/2025).

[28] Encarnación G. Víllora, Dongsheng Yuan, Kiyoshi Shimamura, CeF_3 single crystals for UV-VIS-IR optical isolators, Int. J. Appl. Ceram. Technol. (ISSN: 1744-7402) 20 (4) (2023) 2047–2054, http://dx.doi.org/10.1111/ijac.14398, URL: https://onlinelibrary.wiley.com/doi/abs/10.1111/ijac.14398. (visited on 03/13/2025).

[29] Dongsheng Yuan, Encarnación G. Víllora, Kiyoshi Shimamura, Regular hexagonal-prism microvoids in CeF_3 single crystals, J. Cryst. Growth (ISSN: 0022-0248) 558 (2021) 126024, http://dx.doi.org/10.1016/j.jcrysgro.2020.126024, URL: https://www.sciencedirect.com/science/article/pii/S0022024820305479. (visited on 03/13/2025).

[30] Oswald Kubaschewski, C.B. Alcock, Metallurgical Thermochemistry, fifth ed., Pergamon Press, ISBN: 978-0-08-020897-8, 1979, p. 468.

[31] K.A. Strain, J. Hough, N.A. Robertson, K. Skeldon, Measurement of the absorptance of fused silica at λ=514.5 nm, Opt. Commun. (ISSN: 0030-4018) 117 (5) (1995) 385–388, http://dx.doi.org/10.1016/0030-4018(95)00213-R, URL: https://www.sciencedirect.com/science/article/pii/003040189500213R. (visited on 03/13/2025).